

Scaling analyses of the spectral dimension in 3-dimensional causal dynamical triangulations

Joshua H. Cooperman¹

¹*15 Pond Drive West, Rhinebeck, New York 12572, United States*

October 7, 2018

Abstract

The spectral dimension measures the dimensionality of a space as witnessed by a diffusing random walker. Within the causal dynamical triangulations approach to the quantization of gravity [9, 10, 14], the spectral dimension exhibits novel scale-dependent dynamics: reducing towards a value near 2 on sufficiently small scales, matching closely the topological dimension on intermediate scales, and decaying in the presence of positive curvature on sufficiently large scales [12, 13, 16, 20, 24, 26, 28]. I report the first comprehensive scaling analysis of the small-to-intermediate scale spectral dimension for the test case of the causal dynamical triangulations of 3-dimensional Einstein gravity. I find that the spectral dimension scales trivially with the diffusion constant. I find that the spectral dimension is completely finite in the infinite volume limit, and I argue that its maximal value is exactly consistent with the topological dimension of 3 in this limit. I find that the spectral dimension reduces further towards a value near 2 as this case's bare coupling approaches its phase transition, and I present evidence against the conjecture that the bare coupling simply sets the overall scale of the quantum geometry [11]. On the basis of these findings, I advance a tentative physical explanation for the dynamical reduction of the spectral dimension observed within causal dynamical triangulations: branched polymeric quantum geometry on sufficiently small scales. My analyses should facilitate attempts to employ the spectral dimension as a physical observable with which to delineate renormalization group trajectories in the hope of taking a continuum limit of causal dynamical triangulations at a nontrivial ultraviolet fixed point [3, 6, 21, 22, 26].

1 Introduction

The causal dynamical triangulations approach to the quantization of gravity produced the first significant indication that spacetime dimensionality dynamically reduces on sufficiently small length scales [12]. Specifically, numerical measurements revealed the spectral dimension decreasing from a value of approximately 4 on intermediate scales to a value of approximately 2 on sufficiently small scales [12, 13, 28]. More recent such measurements, performed at different values of the bare couplings, showed dynamical reduction towards a value closer to $\frac{3}{2}$ [26]. Evidence for dynamical dimensional reduction has subsequently emerged from several other approaches to the quantization of gravity [18].

Although the original paper documenting dynamical dimensional reduction dates back more than a decade [12], only recently did Coumbe and Jurkiewicz perform a more thorough study [26]. I now report a comprehensive study, including several scaling analyses not considered by Coumbe and Jurkiewicz, for the case of the causal dynamical triangulations of 3-dimensional Einstein gravity. This computationally simpler model reproduces all of the known phenomenology of the causal dynamical triangulations of 4-dimensional Einstein gravity, excepting certain aspects of the latter model's phase structure [11, 15, 16, 17, 20, 24, 25, 28]. Indeed, as the results reported below demonstrate, the former model's spectral dimension exhibits the behavior of the latter model's spectral dimension even more closely than previously appreciated. I study the 3-dimensional model as an informative prelude to the more realistic 4-dimensional model.

In the case of the causal dynamical triangulations of 3-dimensional Einstein gravity, numerical measurements of the spectral dimension involve three parameters: the diffusion constant ρ characterizing random walks on causal triangulations, the number N_3 of 3-simplices used to construct causal triangulations, and the

bare coupling k_0 of the Euclidean Regge action for causal triangulations. After introducing the causal dynamical triangulations approach in section 2 and the spectral dimension in section 3, I study the dependence of the spectral dimension on each of these parameters in section 4. Investigating variation of the diffusion constant ρ in subsection 4.1, I show that the diffusion constant ρ trivially rescales the spectral dimension's diffusion time dependence. Investigating variation of the number N_3 of 3-simplices in subsection 4.2, I show that the spectral dimension remains finite in the infinite volume limit, as previously expected [12, 13, 26], but slightly overshoots the topological dimension of 3, as previously observed [16]. Investigating variation of the bare coupling k_0 in subsection 4.3, I show that the amount of dimensional reduction increases towards the model's phase transition, just as occurs within the 4-dimensional model [26]. I also show in subsection 4.3 that numerical measurements of the spectral dimension for different values of k_0 do not differ simply by rescaling as a function of k_0 , casting doubt on the conjecture of Ambjørn, Jurkiewicz, and Loll that k_0 simply sets an overall scale [11]. I discuss consequences of the analyses of section 4 in section 5. I propose a way in which to reconcile the spectral dimension with the topological dimension in the infinite volume limit. I hypothesize a physical explanation for the spectral dimension's dynamical reduction. I argue that, beyond further characterizing the spectral dimension and its dynamical reduction, the analyses of section 4 should prove valuable for employing the spectral dimension to delineate renormalization group flows [3, 21, 22, 26]. Following the treatment of [20], I provide an explicit explanation of my method for estimating the spectral dimension and its error in appendix A.

2 Causal dynamical triangulations

Causal dynamical triangulations is an approach to the nonperturbative quantization of classical theories of gravity based on a particular lattice regularization of the path integral [9, 10, 14]. Within this approach one studies the regularized gravitational transition amplitudes

$$\mathcal{A}_\Sigma[\Gamma] = \sum_{\substack{\mathcal{T}_c \cong [0,1] \times \Sigma \\ \mathcal{T}_c|_{\partial\mathcal{T}_c} = \Gamma}} \mu(\mathcal{T}_c) e^{i\mathcal{S}_{\text{cl}}[\mathcal{T}_c]/\hbar} \quad (2.1)$$

defined *via* path summation over causal triangulations \mathcal{T}_c . A causal triangulation is a piecewise-Minkowski simplicial manifold possessing a global foliation by spacelike hypersurfaces all of the topology Σ ; accordingly, a causal triangulation has the spacetime topology $[0, 1] \times \Sigma$. One constructs a causal triangulation by appropriately gluing together N_D causal D -simplices, each a simplicial piece of D -dimensional Minkowski spacetime with spacelike edges of squared invariant length a^2 and timelike edges of squared invariant length $-\alpha a^2$. a is the lattice spacing, and α is a positive constant. Each causal D -simplex spans two adjacent spacelike hypersurfaces of the global foliation. One specifies $\mathcal{A}_\Sigma[\Gamma]$ by choosing the triangulation Γ of the boundary $\partial\mathcal{T}_c$ of \mathcal{T}_c , setting the measure $\mu(\mathcal{T}_c)$ equal to the inverse of the order of the automorphism group of \mathcal{T}_c , and forming the translation $\mathcal{S}_{\text{cl}}[\mathcal{T}_c]$ of the classical action $S_{\text{cl}}[\mathbf{g}]$ into the Regge calculus of causal triangulations.

In the case of three dimensions, analytic calculations of $\mathcal{A}_\Sigma[\Gamma]$ are not currently possible. To study the quantum theory of gravity defined by the transition amplitudes of equation (2.1), one therefore employs numerical techniques, specifically Monte Carlo methods. To enable the application of such methods, one performs a Wick rotation of each causal triangulation by analytically continuing α to $-\alpha$ through the lower-half complex plane. One then numerically generates an ensemble of causal triangulations representative of those contributing to the partition function

$$\mathcal{Z}_\Sigma[\Gamma] = \sum_{\substack{\mathcal{T}_c \cong [0,1] \times \Sigma \\ \mathcal{T}_c|_{\partial\mathcal{T}_c} = \Gamma}} \mu(\mathcal{T}_c) e^{-\mathcal{S}_{\text{cl}}^{(E)}[\mathcal{T}_c]/\hbar}, \quad (2.2)$$

obtained *via* the Wick rotation from the path summation in equation (2.1). $\mathcal{S}_{\text{cl}}^{(E)}[\mathcal{T}_c]$ is the resulting Euclidean action. Typically, one runs numerical simulations at a fixed number N_D of causal D -simplices and a fixed number T of leaves of the global foliation. Taking $S_{\text{cl}}[\mathbf{g}]$ as that of 3-dimensional Einstein gravity for 2-sphere spatial topology Σ and transforming $[0, 1]$ into the 1-sphere by periodic identification,

$$\mathcal{S}_{\text{cl}}^{(E)}[\mathcal{T}_c] = -k_0 N_0 + k_3 N_3 \quad (2.3)$$

in which the bare couplings k_0 and k_3 are functions of the bare Newton constant G_0 , the bare cosmological constant Λ_0 , and the lattice spacing a , and N_0 is the number of 0-simplices [10]. The numerical value of α is irrelevant in three dimensions; moreover, k_3 is not independent of k_0 as the partition function (2.2) for fixed N_3 is only well-defined at the critical value $k_3^c(k_0, N_3)$.

For the action (2.3) the partition function (2.2) exhibits two phases of quantum geometry separated by a first-order transition at the critical value $k_0^c \approx 3.3$ of k_0 [11, 28].¹ I consider exclusively the so-labeled phase C, a condensate of 3-simplices that exhibits de Sitter-like properties on sufficiently large scales and dynamical reduction of the spectral dimension on sufficiently small scales [11, 15, 16, 17, 20, 24, 25, 28]. I consider only the condensate itself, excising the so-called stalk—a component of each causal triangulation now recognized as a numerical artifact [25]—prior to numerical measurement of the spectral dimension. I provide a graphical representation of the condensate and the stalk in figure 2.1. To distinguish the condensate from the stalk,

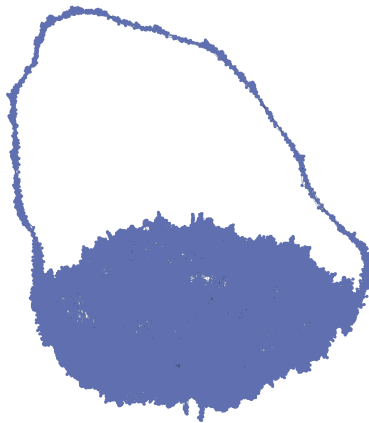


Figure 2.1: A graphical representation of a dual causal triangulation within phase C. The global foliation advances around the loop; the condensate and the stalk are self-evident.

I analyze the evolution of the discrete spatial 2-volume in the global foliation as described, for instance, in [15, 25]. I return to the other phase, so-labeled A, in section 5.

Ultimately, one hopes to remove the lattice regularization of causal triangulations by finding a continuum limit in which the lattice spacing vanishes while expectation values of physical observables remain finite. Typically, the existence of such a continuum limit is contingent upon the existence of an ultraviolet fixed point of the renormalization group, and the existence of such a fixed point is contingent upon the existence of a second-order (or higher-order) phase transition. Since the causal dynamical triangulations of 3-dimensional Einstein gravity lacks such phase transitions, one would not expect this model to possess a continuum limit and, moreover, that taking this continuum limit requires no tuning of k_0 [11]. I return to their argument in subsection 4.3. I explain in section 5 that the analyses of the spectral dimension reported in section 4 will in any case prove instructive for attempts to find a continuum limit of the causal dynamical triangulations of 4-dimensional Einstein gravity, a model that possess at least one second-order phase transition [1, 2, 7, 8]. Furthermore, one hopes to demonstrate an Osterwalder-Schrader-type theorem for causal dynamical triangulations to understand the import of numerical results derived from the partition function (2.2) for the transition amplitude (2.1).

3 Spectral dimension

Several measures of dimensionality, including the so-called spectral dimension, are based on properties of random walks. Consider a random walker diffusing through a D -dimensional Riemannian manifold \mathcal{M} with

¹As implemented numerically, my definition of k_0 differs by a factor of 2 from that of [11].

metric \mathbf{g} . The heat equation,

$$\frac{\partial}{\partial s} K(\mathbf{x}, \mathbf{x}', s) = \wp \nabla_{\mathbf{g}}^2 K(\mathbf{x}, \mathbf{x}', s), \quad (3.1)$$

governs the random walker's diffusion. Subject to the initial condition

$$K(\mathbf{x}, \mathbf{x}', 0) = \sqrt{\det \mathbf{g}(\mathbf{x})} \delta^{(D)}(\mathbf{x} - \mathbf{x}') \quad (3.2)$$

specifying the walker's initial location, $K(\mathbf{x}, \mathbf{x}', s)$ is the probability of diffusion from location \mathbf{x} to location \mathbf{x}' in diffusion time s for diffusion constant \wp . The return probability,

$$P(s) = \frac{1}{\text{vol}(\mathcal{M})} \int_{\mathcal{M}} d^D \mathbf{x} \sqrt{\det \mathbf{g}(\mathbf{x})} K(\mathbf{x}, \mathbf{x}, s), \quad (3.3)$$

is the probability that the walker returns to its initial location in diffusion time s (irregardless of its initial location). One defines the spectral dimension $D_{\mathfrak{s}}(s)$ as follows:

$$D_{\mathfrak{s}}(s) = -2 \frac{d \ln P(s)}{d \ln s}. \quad (3.4)$$

$D_{\mathfrak{s}}(s)$ quantifies the scaling of $P(s)$ with s ; the factor of -2 ensures that

$$\lim_{s \rightarrow 0} D_{\mathfrak{s}}(s) = D, \quad (3.5)$$

yielding agreement of $D_{\mathfrak{s}}(0)$ with the topological dimension D . The content of equation (3.5) constitutes a primary reason for regarding $D_{\mathfrak{s}}(s)$ as a measure of dimension. Of course, any scale-dependent measure of dimension should yield D for $s = 0$ since a sufficiently small neighborhood of a Riemannian manifold is isomorphic to Euclidean space. A sufficiently large neighborhood of a Riemannian manifold is generically not isomorphic to Euclidean space, in which case $D_{\mathfrak{s}}(s) \neq D$ for $s \neq 0$. $D_{\mathfrak{s}}(s)$ provides a measure of the dimensionality of \mathcal{M} on the scale specified by s .²

I now adapt the above definition of the spectral dimension to the setting of causal triangulations [12, 13, 16]. Consider a random walker diffusing through a D -dimensional Wick-rotated causal triangulation \mathcal{T}_c . The integrated heat equation takes the form

$$\mathcal{K}(\mathfrak{s}, \mathfrak{s}', \sigma + 1) = (1 - \rho) \mathcal{K}(\mathfrak{s}, \mathfrak{s}', \sigma) + \frac{\rho}{N(\mathcal{N}(\mathfrak{s}'))} \sum_{\mathfrak{s}'' \in \mathcal{N}(\mathfrak{s}')} \mathcal{K}(\mathfrak{s}, \mathfrak{s}'', \sigma). \quad (3.6)$$

Subject to the initial condition

$$\mathcal{K}(\mathfrak{s}, \mathfrak{s}', 0) = \delta_{\mathfrak{s}\mathfrak{s}'} \quad (3.7)$$

specifying the walker's initial D -simplex, $\mathcal{K}(\mathfrak{s}, \mathfrak{s}', \sigma)$ is the probability of diffusion from D -simplex \mathfrak{s} to D -simplex \mathfrak{s}' in σ diffusion time steps for diffusion constant ρ . $\mathcal{N}(\mathfrak{s}')$ is the set of $N(\mathcal{N}(\mathfrak{s}'))$ D -simplices neighboring the simplex \mathfrak{s}' . The return probability,

$$\mathcal{P}(\sigma) = \frac{1}{N_3(\mathcal{T}_c)} \sum_{\mathfrak{s} \in \mathcal{T}_c} \mathcal{K}(\mathfrak{s}, \mathfrak{s}, \sigma), \quad (3.8)$$

is the probability that the walker returns to its initial D -simplex in σ diffusion time steps (irregardless of its initial D -simplex). One defines the spectral dimension $\mathcal{D}_{\mathfrak{s}}(\sigma)$ as follows:

$$\mathcal{D}_{\mathfrak{s}}(\sigma) = -2 \frac{d \ln \mathcal{P}(\sigma)}{d \ln \sigma} \quad (3.9)$$

for appropriate finite differences. In particular, expanding the logarithmic derivative in equation (3.9),

$$\mathcal{D}_{\mathfrak{s}}(\sigma) = -\frac{\sigma}{\mathcal{P}(\sigma)} [\mathcal{P}(\sigma + 1) - \mathcal{P}(\sigma - 1)] \quad (3.10)$$

²In the mathematics literature the spectral dimension is typically defined as $\lim_{s \rightarrow 0} D_{\mathfrak{s}}(s)$.

to lowest order in $\Delta\sigma = 1$.

I finally adapt the above definition of the spectral dimension to an ensemble of causal triangulations. Consider an ensemble of $N(\mathcal{T}_c)$ D -dimensional Wick-rotated causal triangulations \mathcal{T}_c . The expectation value of $\mathcal{D}_s(\sigma)$ in the quantum state (2.2) is defined as follows:

$$\mathbb{E}[\mathcal{D}_s(\sigma)] = \frac{1}{\mathcal{Z}[\Gamma]} \sum_{\substack{\mathcal{T}_c \cong [0,1] \times \Sigma \\ \mathcal{T}_c|_{\partial\mathcal{T}_c} = \Gamma}} \mu(\mathcal{T}_c) e^{-S_{\text{cl}}^{(\text{E})}[\mathcal{T}_c]/\hbar} \mathcal{D}_s^{(\mathcal{T}_c)}(\sigma). \quad (3.11)$$

I estimate $\mathbb{E}[\mathcal{D}_s(\sigma)]$ by the ensemble average

$$\langle \mathcal{D}_s(\sigma) \rangle = \frac{1}{N(\mathcal{T}_c)} \sum_{j=1}^{N(\mathcal{T}_c)} \mathcal{D}_s^{(\mathcal{T}_c^{(j)})}(\sigma). \quad (3.12)$$

$\langle \mathcal{D}_s(\sigma) \rangle$ provides a measure of the dimensionality of the quantum geometry on the scale corresponding to σ defined by an ensemble of causal triangulations. I report numerical measurements of $\langle \mathcal{D}_s(\sigma) \rangle$ for several ensembles of causal triangulations within phase C in section 4.

4 Scaling analyses

Three parameters—the diffusion constant ρ , the number N_3 of 3-simplices, and the bare coupling k_0 —enter into a numerical measurement of the ensemble average spectral dimension $\langle \mathcal{D}_s(\sigma) \rangle$.³ I explore the dependence of $\langle \mathcal{D}_s(\sigma) \rangle$ on ρ for fixed N_3 and k_0 in subsection 4.1, the dependence of $\langle \mathcal{D}_s(\sigma) \rangle$ on N_3 for fixed ρ and k_0 in subsection 4.2, and the dependence of $\langle \mathcal{D}_s(\sigma) \rangle$ on k_0 for fixed ρ and N_3 in subsection 4.3. In each of these explorations, I look for evidence of scaling of $\langle \mathcal{D}_s(\sigma) \rangle$ with the parameter being varied.

The exploration of subsection 4.2 is a standard finite-size scaling analysis. I present numerical measurements of $\langle \mathcal{D}_s(\sigma) \rangle$ for increasing values of N_3 from which I attempt to extrapolate towards the infinite volume limit $N_3 \rightarrow \infty$. As I discuss further in subsection 4.2 below, one only expects to obtain a nontrivial continuum limit in conjunction with the infinite volume limit. Accordingly, finiteness of $\langle \mathcal{D}_s(\sigma) \rangle$ in the infinite volume limit, which I determine through this finite-size scaling analysis, may be necessary for finiteness of $\langle \mathcal{D}_s(\sigma) \rangle$ in a continuum limit.

4.1 Dependence on the diffusion constant ρ

I first explore the dependence of $\langle \mathcal{D}_s(\sigma) \rangle$ on ρ holding fixed k_0 and N_3 . Equation (3.1) implies a trivial dependence: since the diffusion constant \wp —or, more precisely, \wp^{-1} —enters as a constant factor multiplying the diffusion time s , \wp simply rescales s . This conclusion does not follow straightforwardly from equation (3.6), and computing the expectation value of $\mathcal{D}_s(\sigma)$ with respect to the partition function (2.2) further complicates predicting this dependence. I have instead performed measurements of $\langle \mathcal{D}_s(\sigma) \rangle$ for five values of ρ at fixed k_0 and N_3 to determine its dependence on ρ . I display these measurements in figure 4.1.

The plots in figure 4.1 exhibit the characteristic behavior of $\langle \mathcal{D}_s(\sigma) \rangle$ within phase C. The case of $\rho = 0.8$ (orange, upright triangles) provides the clearest illustration. As σ increases from a value of order 10 to a value of order 100, $\langle \mathcal{D}_s(\sigma) \rangle$ increases monotonically from a value of approximately 2.5 to a value of approximately 2.65. Read in reverse, this is the phenomenon of dynamical reduction of $\langle \mathcal{D}_s(\sigma) \rangle$, first reported in [12]. While figure 4.6 below attests that $\langle \mathcal{D}_s(\sigma) \rangle$ dynamically reduces to its minimal value $\langle \mathcal{D}_s \rangle_{\text{min}}$ of approximately 2.5 irregardless of the value of N_3 , figures 4.11, 4.12, and 4.15 below attest that $\langle \mathcal{D}_s \rangle_{\text{min}}$ depends on the value of k_0 .⁴ Previous studies have attested [12, 13, 16, 20, 26] and figure 4.6 below further attests that sufficiently small values of N_3 depress the maximal value $\langle \mathcal{D}_s \rangle_{\text{max}}$ of $\langle \mathcal{D}_s(\sigma) \rangle$ —in this case approximately 2.65—below the value of the topological dimension—in this case 3.⁵ As σ subsequently increases beyond a value of order

³One also specifies the number T of leaves of the global foliation, but the number of leaves within the condensate is dynamically determined, so the dependence of $\langle \mathcal{D}_s(\sigma) \rangle$ on T is quite weak.

⁴I exclude the (presumably) unphysically small values of $\langle \mathcal{D}_s(\sigma) \rangle$ for very small values of σ ($\sigma < 15$ for $\rho = 0.2$, $\sigma < 4$ for $\rho = 0.4$, $\sigma < 9$ for $\rho = 0.8$).

⁵I exclude the (presumably) unphysically large values of $\langle \mathcal{D}_s(\sigma) \rangle$ for very small σ ($\sigma < 3$ for $\rho = 0.6$, $\sigma < 6$ for $\rho = 0.8$, $\sigma < 18$ for $\rho = 1$).

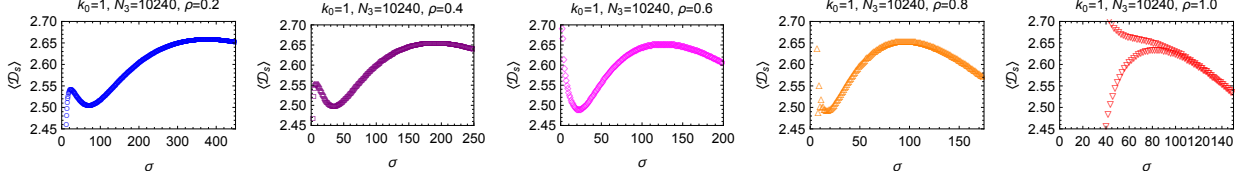


Figure 4.1: The ensemble average spectral dimension $\langle \mathcal{D}_s \rangle$ as a function of diffusion time σ for diffusion constants $\rho = 0.2, \rho = 0.4, \rho = 0.6, \rho = 0.8,$ and $\rho = 1.0$ (from left to right) for $k_0 = 1.00, N_3 = 9267,$ and $T = 64.$

100, $\langle \mathcal{D}_s(\sigma) \rangle$ decreases monotonically towards a value of 0 [16]. In the cases of $\rho = 0.2, \rho = 0.4,$ and $\rho = 0.6,$ $\langle \mathcal{D}_s(\sigma) \rangle$ exhibits additional structure for very small σ : as σ increases from a value of order 1 to a value of order 10, $\langle \mathcal{D}_s(\sigma) \rangle$ decreases slightly from a value of approximately 2.55 to a value of approximately 2.5. I have yet to ascertain whether or not this decrease is a physical phenomenon; the physical explanation for the spectral dimension's dynamical reduction that I propose in section 5 implies that this decrease is not a physical phenomenon.

The dynamical reduction of $\langle \mathcal{D}_s(\sigma) \rangle$ is obscured for $\rho = 1$ because random walks of even and odd σ for $\sigma < 100$ yield disparate estimates for $\langle \mathcal{D}_s(\sigma) \rangle$. As Benedetti and Henson first observed [16], and as figure 4.1 attests, choosing $\rho < 1$ significantly smooths the oscillations in $\langle \mathcal{D}_s(\sigma) \rangle$. To render $\langle \mathcal{D}_s(\sigma) \rangle$ for $\rho = 1$ useful for subsequent comparisons with $\langle \mathcal{D}_s(\sigma) \rangle$ for $\rho < 1,$ I compute an interpolated value $\langle \mathcal{D}_s(\sigma) \rangle_{\text{int}}$ of $\langle \mathcal{D}_s(\sigma) \rangle$ for $\rho = 1$ using a straightforward averaging technique:

$$\langle \mathcal{D}_s(\sigma) \rangle_{\text{int}} = \frac{1}{4} [\langle \mathcal{D}_s(\sigma - 1) \rangle + 2\langle \mathcal{D}_s(\sigma) \rangle + \langle \mathcal{D}_s(\sigma + 1) \rangle] \quad (\rho = 1). \quad (4.1)$$

Alongside $\langle \mathcal{D}_s(\sigma) \rangle$ for $\rho = 0.2, \rho = 0.4, \rho = 0.6,$ and $\rho = 0.8,$ I plot $\langle \mathcal{D}_s(\sigma) \rangle_{\text{int}}$ (for $\rho = 1$) in figure 4.2. The

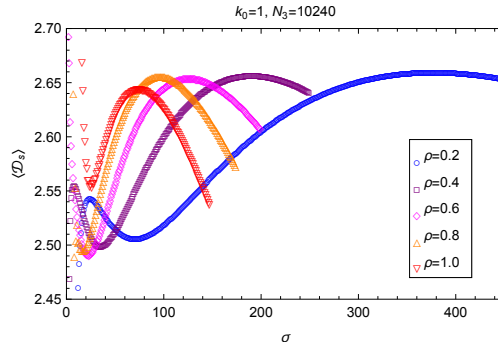


Figure 4.2: The ensemble average spectral dimension $\langle \mathcal{D}_s \rangle$ as a function of diffusion time σ for five values of the diffusion constant ρ for $k_0 = 1.00, N_3 = 9267,$ and $T = 64.$

dynamical reduction of $\langle \mathcal{D}_s(\sigma) \rangle_{\text{int}}$ is now evident.

I now turn to the dependence of $\langle \mathcal{D}_s(\sigma) \rangle$ on $\rho.$ I wish to determine the relationship between measurements of $\langle \mathcal{D}_s(\sigma) \rangle$ performed for different values of $\rho.$ I focus on the maximum of $\langle \mathcal{D}_s(\sigma) \rangle$ as a clearly identifiable point of comparison. I first plot $\langle \mathcal{D}_s \rangle_{\text{max}}$ as a function of ρ in figure 4.3, which shows that $\langle \mathcal{D}_s \rangle_{\text{max}}$ is a constant function of ρ (up to measurement errors as computed in appendix A). (Although this last statement includes $\langle \mathcal{D}_s \rangle_{\text{max}}$ for $\rho = 1,$ I discount to some extent the value of $\langle \mathcal{D}_s \rangle_{\text{max}}$ for $\rho = 1$ since this value results from the naive interpolation (4.1).) I next plot $\sigma_{\text{max}},$ the value of σ at which $\langle \mathcal{D}_s(\sigma) \rangle$ attains the value $\langle \mathcal{D}_s \rangle_{\text{max}},$ as a function of ρ in figure 4.1(a). In light of the regular decrease of σ_{max} with ρ exhibited in figure 4.1(a), I test for scaling of σ_{max} with ρ by plotting $\ln \sigma_{\text{max}}$ as a function of $\ln \rho$ in figure 4.1(b). The plot in figure 4.1(b) clearly exhibits scaling of σ_{max} with $\rho.$ Fitting a line to $\ln \sigma_{\text{max}}$ as a function of $\ln \rho,$ I obtain

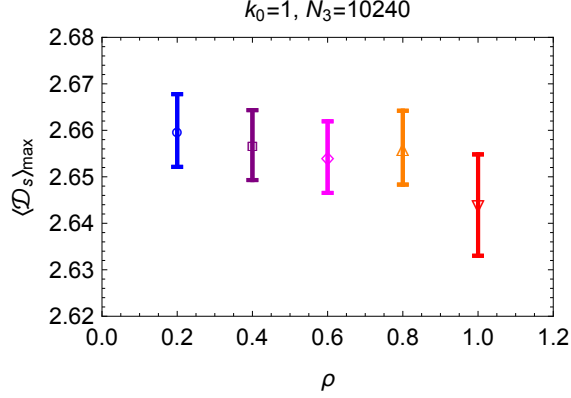


Figure 4.3: The maximal value $\langle \mathcal{D}_s \rangle_{\max}$ of the ensemble average spectral dimension $\langle \mathcal{D}_s(\sigma) \rangle$ as a function of the diffusion constant ρ for $k_0 = 1.00$, $N_3 = 9267$, and $T = 64$.

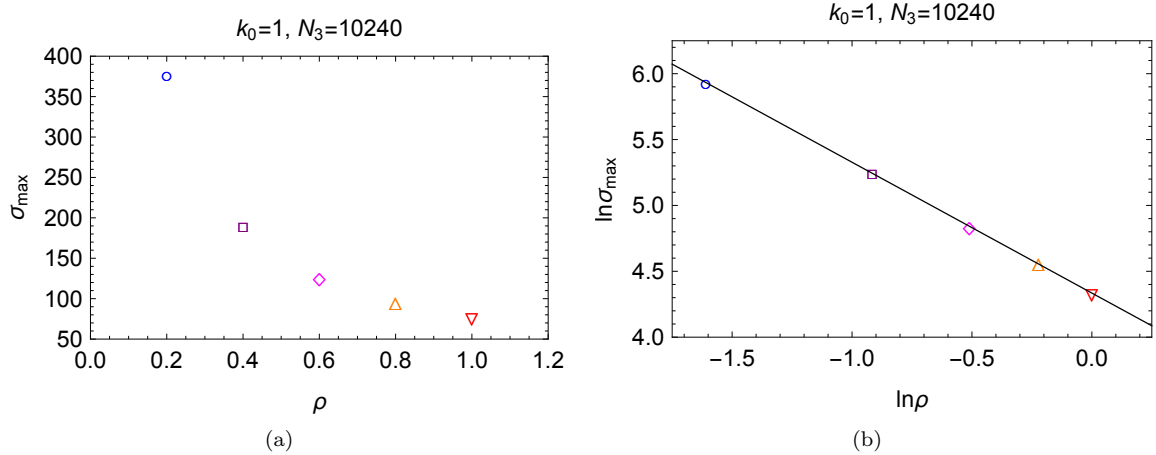


Figure 4.4: (a) The diffusion time σ_{\max} as a function of the diffusion constant ρ for $k_0 = 1.00$, $N_3 = 9267$, and $T = 64$. (b) The logarithm $\ln \sigma_{\max}$ of the diffusion time σ_{\max} as a function of the logarithm $\ln \rho$ of the diffusion constant ρ for $k_0 = 1.00$, $N_3 = 9267$, and $T = 64$ overlain with the linear least-squares fit $\ln \sigma_{\max} = 4.33 - 0.99 \ln \rho$.

a slope of -0.99 . Evidently, $\langle \mathcal{D}_s(\sigma) \rangle$ depends trivially on ρ , matching the expectation from equation (3.1). Applying this scaling to $\langle \mathcal{D}_s(\sigma) \rangle$, I plot $\langle \mathcal{D}_s(\rho\sigma) \rangle$ in figure 4.5. The overlap of $\langle \mathcal{D}_s(\rho\sigma) \rangle$ for the five values of ρ is clear.

4.2 Dependence on the number N_3 of 3-simplices

I next explore the dependence of $\langle \mathcal{D}_s(\sigma) \rangle$ on N_3 holding fixed k_0 and ρ . I have performed measurements of $\langle \mathcal{D}_s(\sigma) \rangle$ for seven values of N_3 ranging from 1×10^5 to 2×10^6 at fixed k_0 and ρ to determine its dependence on N_3 . I display these measurements in figure 4.6.

I again focus on the maximum of $\langle \mathcal{D}_s(\sigma) \rangle$ as a clearly identifiable point of comparison. I first plot $\langle \mathcal{D}_s \rangle_{\max}$ as a function of N_3 in figure 4.7. Previous studies indicate that $\langle \mathcal{D}_s \rangle_{\max}$ approaches the topological dimension of 3 from below in the infinite volume limit, possibly slightly overshooting [16].⁶ The measurements of $\langle \mathcal{D}_s \rangle_{\max}$ in figure 4.7 corroborate these studies: $\langle \mathcal{D}_s \rangle_{\max}$ approaches and slightly overshoots 3 as N_3 increases. Indeed, a value of 3 for $\langle \mathcal{D}_s \rangle_{\max}$ does not fall within the range of the measurement errors for

⁶ $\langle \mathcal{D}_s \rangle_{\max}$ approaches the topological dimension of 4 from below in the infinite volume limit within phase C of the causal dynamical triangulations of (3 + 1)-dimensional Einstein gravity [12, 13, 26].

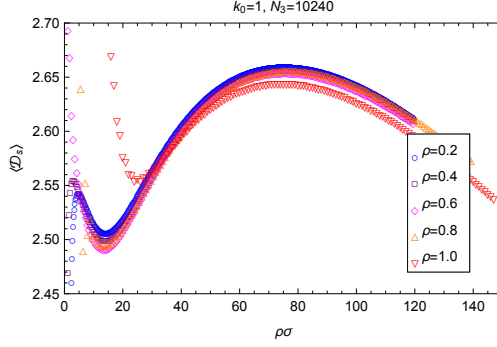


Figure 4.5: The ensemble average spectral dimension $\langle \mathcal{D}_s \rangle$ as a function of the scaled diffusion time $\rho\sigma$ for five values of the diffusion constant ρ for $k_0 = 1.00$, $N_3 = 9267$, and $T = 64$.

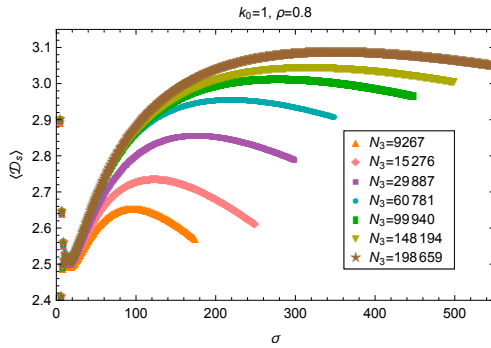


Figure 4.6: The ensemble average spectral dimension $\langle \mathcal{D}_s \rangle$ as a function of the diffusion time σ for seven values of the number N_3 of 3-simplices (within the condensate) for $k_0 = 1.00$ and $\rho = 0.8$.

the three largest values of N_3 . The plot in figure 4.7 also indicates that $\langle \mathcal{D}_s \rangle_{\max}$ continues to increase for $N_3 > 2 \times 10^6$, so the extent of the overshoot in the infinite volume limit may well be more than 0.08. I wish to determine if $\langle \mathcal{D}_s \rangle_{\max}$ is at least finite in the infinite volume limit. In light of the regular increase of $\langle \mathcal{D}_s \rangle_{\max}$ with N_3 exhibited in figure 4.7, I test for scaling of $\langle \mathcal{D}_s \rangle_{\max}$ with N_3 by plotting $\ln \langle \mathcal{D}_s \rangle_{\max}$ as a function of $\ln N_3$ in figure 4.8(a). Performing a linear least squares fit of $\ln \langle \mathcal{D}_s \rangle_{\max}$ as a function of $\ln N_3$, shown as a black line in figure 4.8(a), I find that

$$\ln \langle \mathcal{D}_s \rangle_{\max} = 0.56 + 0.05 \ln N_3, \quad (4.2)$$

implying that

$$\langle \mathcal{D}_s \rangle_{\max}(N_3) \propto N_3^{0.05}. \quad (4.3)$$

I plot the residuals of this fit as a function of $\ln N_3$ in figure 4.8(b). These residuals clearly show a trend, indicating that $\langle \mathcal{D}_s \rangle_{\max}$ does not increase as a power of N_3 but rather increases as a subpower of N_3 . Since a function $f(x)$ that increases as a subpower of x is finite in the limit $x \rightarrow \infty$, I conclude that $\langle \mathcal{D}_s \rangle_{\max}$ is finite in the infinite volume limit. Moreover, the findings of subsection 4.3 below admit the possibility of making $\langle \mathcal{D}_s \rangle_{\max}$ equal to 3 in the infinite volume limit.

I next plot σ_{\max} as a function of N_3 in figure 4.9. In light of the regular increase of σ_{\max} with N_3 exhibited in figure 4.9, I test for scaling of σ_{\max} with N_3 by plotting $\ln \sigma_{\max}$ as a function of $\ln N_3$ in figure 4.10(a). The plot in figure 4.10(a) shows evidence of scaling of σ_{\max} with N_3 : there is an approximately linear relationship between $\ln \sigma_{\max}$ and $\ln N_3$. Performing a linear least squares fit of $\ln \sigma_{\max}$ as a function of $\ln N_3$, shown as a black line in figure 4.10(a), I find that

$$\ln \sigma_{\max} = 0.78 + 0.42 \ln N_3, \quad (4.4)$$

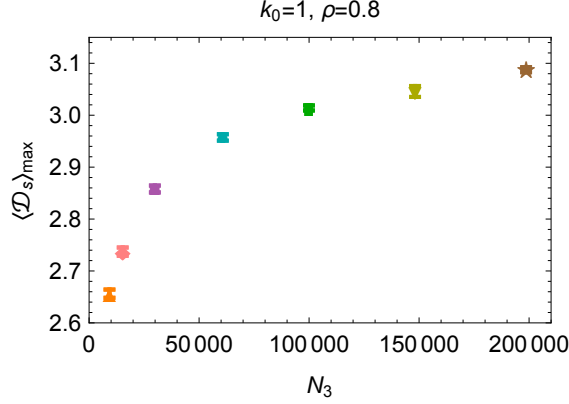


Figure 4.7: The maximal value $\langle \mathcal{D}_s \rangle_{\max}$ of the ensemble average spectral dimension $\langle \mathcal{D}_s(\sigma) \rangle$ as a function of the number N_3 of 3-simplices (within the condensate) for $k_0 = 1.00$ and $\rho = 0.8$.

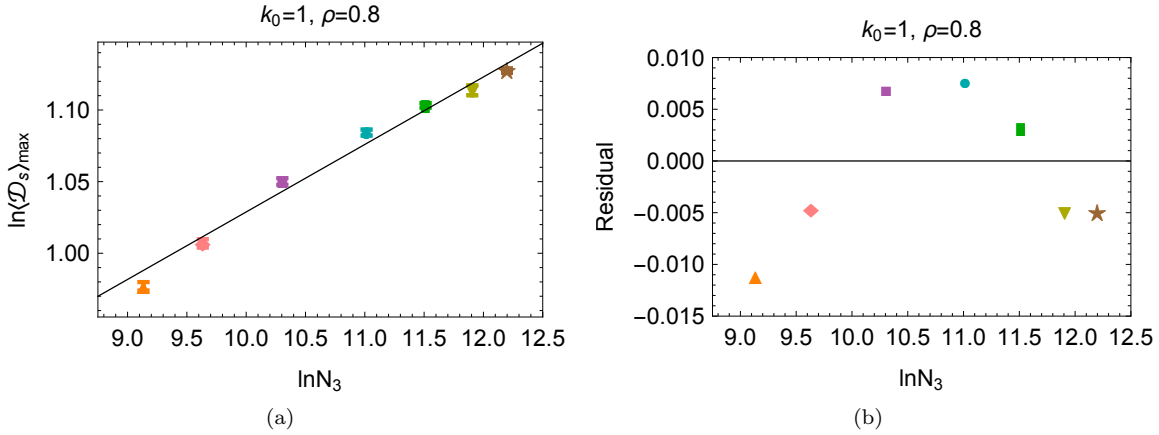


Figure 4.8: **4.8(a)** The logarithm $\ln \langle \mathcal{D}_s \rangle_{\max}$ of the maximal value $\langle \mathcal{D}_s \rangle_{\max}$ of the ensemble average spectral dimension $\langle \mathcal{D}_s(\sigma) \rangle$ as a function of the logarithm $\ln N_3$ of the number N_3 of 3-simplices (within the condensate) for $k_0 = 1.00$ and $\rho = 0.8$ overlain with the linear least-squares fit $\ln \langle \mathcal{D}_s \rangle_{\max} = 0.56 + 0.05 \ln N_3$. **4.8(b)** The residuals of the linear least-squares fit $\ln \langle \mathcal{D}_s \rangle_{\max} = 0.56 + 0.05 \ln N_3$ to the logarithm $\ln \langle \mathcal{D}_s \rangle_{\max}$ of the maximal value $\langle \mathcal{D}_s \rangle_{\max}$ of the ensemble average spectral dimension $\langle \mathcal{D}_s(\sigma) \rangle$ as a function of the logarithm $\ln N_3$ of the number N_3 of 3-simplices (within the condensate) for $k_0 = 1.00$ and $\rho = 0.8$.

implying that

$$\sigma_{\max}(N_3) \propto N_3^{0.42}. \quad (4.5)$$

I plot the residuals of this fit as a function of $\ln N_3$ in figure 4.10(b). Excluding the residual for $N_3 = 60781$ (dark cyan, circle), the residuals show a trend, possibly indicating that σ_{\max} does not increase as a power of N_3 but rather as a subpower of N_3 .

Previous studies possibly suggest that σ_{\max} diverges in the infinite volume limit. These studies have advanced evidence for and made use of the double scaling limit

$$V_3 = \lim_{\substack{N_3 \rightarrow \infty \\ a \rightarrow 0}} C_3 N_3 a^3 \quad (4.6)$$

for the spacetime 3-volume V_3 [11, 16, 17, 24, 25]: in the combination of the infinite volume limit ($N_3 \rightarrow \infty$) and the continuum limit ($a \rightarrow 0$), $C_3 N_3 a^3$ approaches V_3 . C_3 is the effective discrete spacetime 3-volume of a single 3-simplex, so N_3 is essentially the discrete spacetime 3-volume. Assuming that V_3 is fixed (for fixed k_0) and that the double scaling limit (4.6) holds with negligible corrections for finite but sufficiently

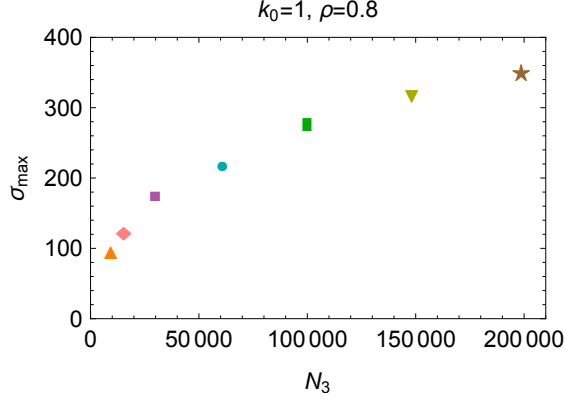


Figure 4.9: The diffusion time σ_{\max} as a function of the number N_3 of 3-simplices (within the condensate) for $k_0 = 1.00$ and $\rho = 0.8$.

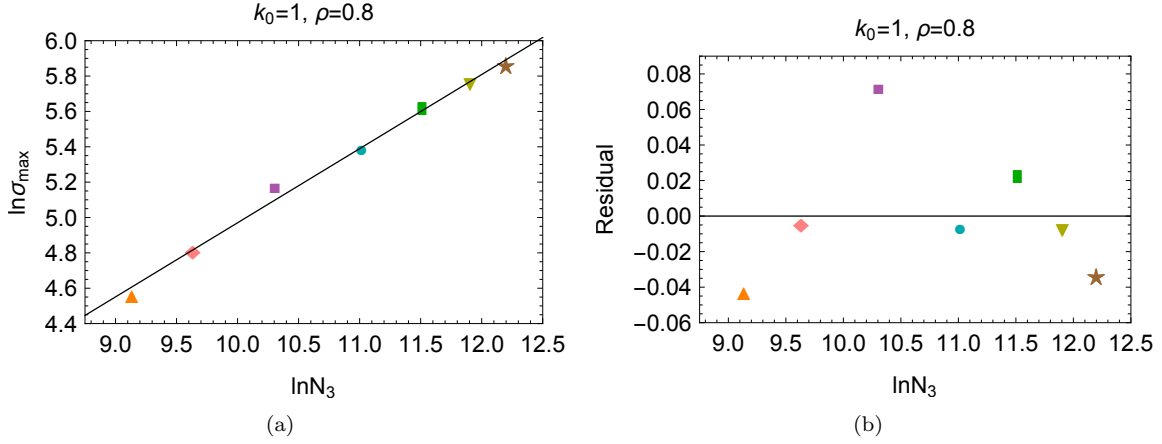


Figure 4.10: (a) The logarithm $\ln \sigma_{\max}$ of the diffusion time σ_{\max} as a function of the logarithm $\ln N_3$ of the number N_3 of 3-simplices (within the condensate) for $k_0 = 1.00$ and $\rho = 0.8$ overlain in black with the linear least squares fit $\ln \sigma_{\max} = 0.78 + 0.42 \ln N_3$. (b) The residuals of the linear least squares fit of the logarithm $\ln \sigma_{\max}$ of the diffusion time σ_{\max} as a function of the logarithm $\ln N_3$ of the number N_3 of 3-simplices (within the condensate) for $k_0 = 1.00$ and $\rho = 0.8$.

large N_3 and finite but sufficiently small a , one concludes that a scales with N_3 as $N_3^{-1/3}$. Accordingly, a discrete quantity associated with units of a^p for some power p (canonically) scales with N_3 as $N_3^{-p/3}$. The diffusion time σ is associated with units of a^2 since the diffusion time s has dimensions of squared length (after absorbing the diffusion constant \wp into s in equation (3.1)). On the basis of the double scaling limit (4.6), one therefore expects σ to scale with N_3 as $N_3^{-2/3}$. Denoting by s_{\max} the fixed value of s at which $D_s(s)$ attains its maximum, one infers that

$$s_{\max} \propto \sigma_{\max}(N_3) a^2. \quad (4.7)$$

The double scaling limit (4.6) and relation (4.7) then dictate that

$$\sigma_{\max}(N_3) \propto N_3^{2/3}, \quad (4.8)$$

implying that σ_{\max} diverges in the infinite volume limit.

The evidence for the double scaling limit (4.6) stems from analysis of large-scale observables [13], and the uses of the double scaling limit (4.6) come in modeling of large-scale observables [15, 16, 17, 24, 25]. For instance, Ambjørn, Jurkiewicz, and Loll originally arrived at the double scaling limit (4.6) by studying

temporal correlations in the discrete spatial volume [13], and Benedetti and Henson applied the double scaling limit (4.6) to the diffusion time in fitting the spectral dimension of deformed de Sitter space to the large-scale ensemble average spectral dimension [16]. Accordingly, I only expect σ to scale with N_3 as $N_3^{-2/3}$ for sufficiently large values of σ , presumably for random walks that probe classical or at least semiclassical regimes.

Evidently, σ_{\max} does not follow the relation (4.8) but scales noncanonically with N_3 . Presumably, for $\sigma < \sigma_{\max}$, σ also scales noncanonically with N_3 . While one should have anticipated noncanonical scaling of σ with N_3 for $\sigma < \sigma_{\max}$ since $\langle \mathcal{D}_s(\sigma) \rangle$ exhibits the quantum-mechanical effect of dynamical dimensional reduction for $\sigma < \sigma_{\max}$, one might have expected σ_{\max} to scale canonically with N_3 since $\langle \mathcal{D}_s(\sigma) \rangle$ attains the topological dimension of 3 on the scale associated with σ_{\max} . This finding is consistent with the analysis of [16] in which canonical scaling of σ with N_3 was only applied for $\sigma > \sigma_{\max}$. The noncanonical scaling of σ_{\max} with N_3 expressed in equation (4.5) suggests that the quantum geometry on the scale associated with σ_{\max} is not as semiclassical as the value of $\langle \mathcal{D}_s(\sigma) \rangle$ suggests.

Numerical measurements of $\langle \mathcal{D}_s(\sigma) \rangle$ for $N_3 > 2 \times 10^5$ should determine whether σ_{\max} is finite or infinite in the infinite volume limit. Despite the inconclusiveness of the above analysis, σ_{\max} presumably diverges in the infinite volume limit taken alone: as N_3 diverges, V_3 diverges, and, as V_3 defines the largest scale characterizing a causal triangulation, any smaller scales can likewise diverge. Conversely, σ_{\max} presumably remains finite in the double scaling limit (4.6), the infinite volume and continuum limits taken together: as N_3 diverges and a vanishes, V_3 remains finite, and, as V_3 defines the largest scale characterizing a causal triangulation, any smaller scales must likewise remain finite.

4.3 Dependence on the bare coupling k_0

I finally explore the dependence of $\langle \mathcal{D}_s(\sigma) \rangle$ on k_0 holding fixed ρ and N_3 . I have performed measurements of $\langle \mathcal{D}_s(\sigma) \rangle$ for five values of k_0 to determine its dependence on k_0 . I display these measurements separately in figure 4.11 and together in figure 4.12. The plots in figures 4.11 and 4.12 show that $\langle \mathcal{D}_s(\sigma) \rangle$ changes

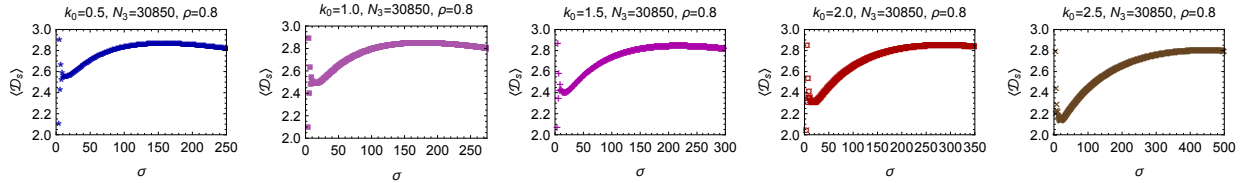


Figure 4.11: The ensemble average spectral dimension $\langle \mathcal{D}_s \rangle$ as a function of the diffusion time σ for bare couplings $k_0 = 0.5$, $k_0 = 1.0$, $k_0 = 1.5$, $k_0 = 2.0$, and $k_0 = 2.5$ for $N_3 = 30850$, $T = 64$, and $\rho = 0.8$.

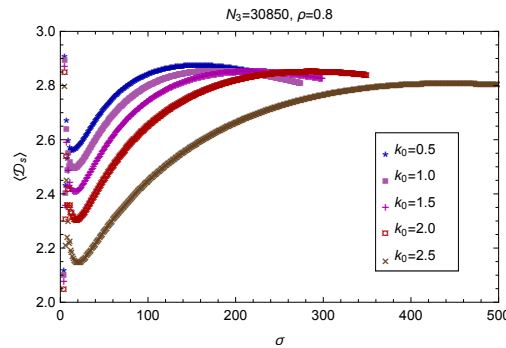


Figure 4.12: The ensemble average spectral dimension $\langle \mathcal{D}_s \rangle$ as a function of the diffusion time σ for five values of the bare coupling k_0 for $N_3 = 30850$, $T = 64$, and $\rho = 0.8$.

with k_0 just as $\langle \mathcal{D}_s(\sigma) \rangle$ changes with the corresponding bare coupling κ_0 within phase C of the causal dynamical triangulations of 4-dimensional Einstein gravity [26]. This constitutes another respect in which the phenomenology of the 3-dimensional model reproduces that of the 4-dimensional model.

I once again focus on the maximum of $\langle \mathcal{D}_s(\sigma) \rangle$ as a clearly identifiable point of comparison. I first plot $\langle \mathcal{D}_s \rangle_{\max}$ as a function of k_0 in figure 4.13. The plot in figure 4.13 shows that $\langle \mathcal{D}_s \rangle_{\max}$ is a constant function

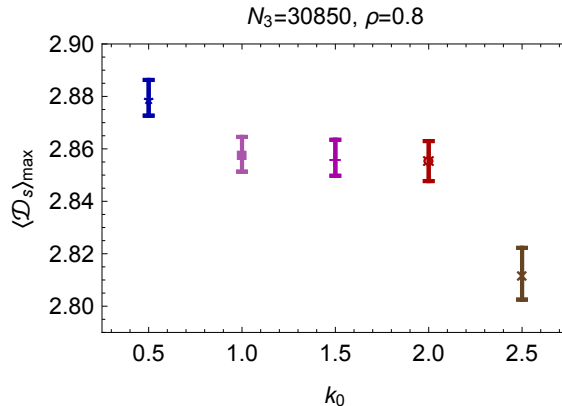


Figure 4.13: The maximal value $\langle \mathcal{D}_s \rangle_{\max}$ of the ensemble average spectral dimension $\langle \mathcal{D}_s(\sigma) \rangle$ as a function of the bare coupling k_0 for $N_3 = 30850$, $T = 64$, and $\rho = 0.8$.

of k_0 (up to measurement errors) for k_0 well within phase C, that $\langle \mathcal{D}_s \rangle_{\max}$ increases as k_0 approaches 0, and that $\langle \mathcal{D}_s \rangle_{\max}$ decreases as k_0 approaches the AC phase transition. Note, though, that, ignoring measurement errors, $\langle \mathcal{D}_s \rangle_{\max}$ decreases monotonically with k_0 , albeit very slowly well within phase C. One might suspect that this decrease of $\langle \mathcal{D}_s \rangle_{\max}$ with k_0 is merely a finite-size effect since the number of 3-simplices within the condensate also decreases with k_0 . (See figure ?? below.) An analysis of the number of 3-simplices within the condensate as a function of k_0 indicates that this suspicion is unsubstantiated (unless proximity to the AC phase transition amplifies the finite-size effect).

I next plot σ_{\max} as a function of k_0 in figure 4.14(a). In light of the regular increase of σ_{\max} with k_0

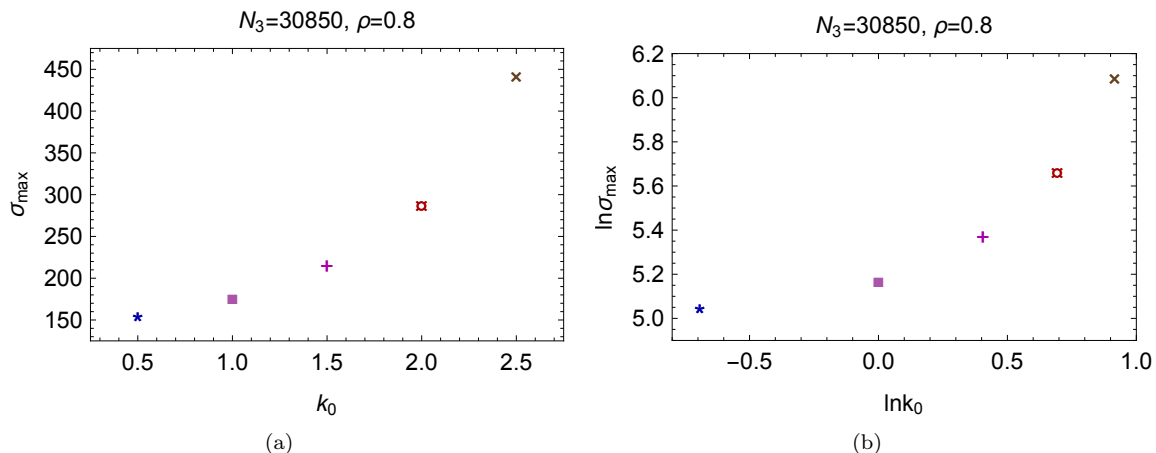


Figure 4.14: (a) The diffusion time σ_{\max} as a function of the bare coupling k_0 for $N_3 = 30850$, $T = 64$, and $\rho = 0.8$. (b) The logarithm $\ln \sigma_{\max}$ of the diffusion time σ_{\max} as a function of the logarithm $\ln k_0$ of the bare coupling k_0 for $N_3 = 30850$, $T = 64$, and $\rho = 0.8$.

exhibited in figure 4.14(a), I test for scaling of σ_{\max} with k_0 by plotting $\ln \sigma_{\max}$ as a function of $\ln k_0$ in figure 4.14(b). The plot in figure 4.14(b) shows that σ_{\max} increases more rapidly with k_0 than as a power of k_0 ; indeed, I conjecture in section 5 that σ_{\max} diverges as k_0 approaches the AC phase transition.

I also consider the minimum of $\langle \mathcal{D}_s(\sigma) \rangle$.⁷ I plot $\langle \mathcal{D}_s \rangle_{\min}$ as a function of k_0 in figure 4.15(a). In light

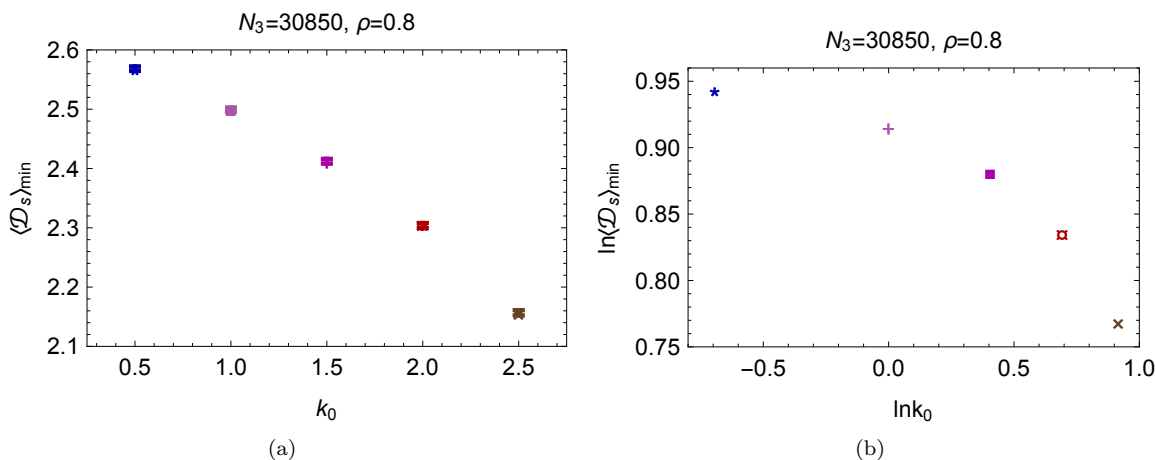


Figure 4.15: (a) The minimal value $\langle \mathcal{D}_s \rangle_{\min}$ of the ensemble average spectral dimension $\langle \mathcal{D}_s \rangle$ as a function of the bare coupling k_0 for $N_3 = 30850$, $T = 64$, and $\rho = 0.8$. (b) The logarithm $\ln \langle \mathcal{D}_s \rangle_{\min}$ of the minimal value $\langle \mathcal{D}_s \rangle_{\min}$ of the ensemble average spectral dimension $\langle \mathcal{D}_s \rangle$ as a function of the logarithm $\ln k_0$ of the bare coupling k_0 for $N_3 = 30850$, $T = 64$, and $\rho = 0.8$.

of the regular decrease of $\langle \mathcal{D}_s \rangle_{\min}$ with k_0 , I test for scaling of $\langle \mathcal{D}_s \rangle_{\min}$ with k_0 by plotting $\ln \langle \mathcal{D}_s \rangle_{\min}$ as a function of $\ln k_0$ in figure 4.15(b). The plot in figure 4.15(b) shows that $\langle \mathcal{D}_s \rangle_{\min}$ decreases more rapidly with k_0 than as a power of k_0 ; nevertheless, I conjecture in section 5 that $\langle \mathcal{D}_s \rangle_{\min}$ approaches a nonzero value at the AC phase transition.

Ambjørn, Jurkiewicz, and Loll conjectured that k_0 only sets the overall scale of the quantum geometry within phase C [11]. Numerical measurements of the temporal evolution of the spatial 2-volume—specifically, the ensemble average number $\langle N_2^{\text{SL}}(\tau) \rangle$ of spacelike 2-simplices as a function of the discrete time coordinate τ labeling the T leaves of the global foliation—constituted their primary evidence. These authors found that, for different values of k_0 , $\langle N_2^{\text{SL}}(\tau) \rangle$ differs only by rescaling by a function of k_0 . I have performed measurements of $\langle N_2^{\text{SL}}(\tau) \rangle$ for the five values of k_0 considered just above. I display these measurements in figure 4.16(a). Rescaling $\langle N_2^{\text{SL}} \rangle$ by a function $f_{\text{SL}}(k_0)$ and τ by a function $f_{\text{TL}}(k_0)$, I confirm the finding of Ambjørn, Jurkiewicz, and Loll: as the plot in figure 4.16(b) shows, for different values of k_0 , $\langle N_2^{\text{SL}}(\tau) \rangle$ differs only by rescaling by the functions $f_{\text{SL}}(k_0)$ and $f_{\text{TL}}(k_0)$.

The numerical measurements of $\langle \mathcal{D}_s(\sigma) \rangle$ depicted in figures 4.11 and 4.12 serve to further test the conjecture of Ambjørn, Jurkiewicz, and Loll. Since the spectral dimension is dimensionless, I do not expect to its value to scale with the hypothetical scale set by k_0 ; since the diffusion time is dimensionful, I do expect its value to scale with the hypothetical scale set by k_0 . Accordingly, rescaling σ by a function $g(k_0)$, I plot $\langle \mathcal{D}_s \rangle$ as a function of $g(k_0)\sigma$ in figure 4.17(a). Rescaling σ alone fails to result in complete overlapping of $\langle \mathcal{D}_s(\sigma) \rangle$ for different values of k_0 . Of course, I expected this failure on the basis of the plot in figure 4.14(a). Rescaling also $\langle \mathcal{D}_s \rangle$ by a function $h(k_0)$, I plot $h(k_0)\langle \mathcal{D}_s \rangle$ as a function of $g(k_0)\sigma$ in figure 4.17(b). Rescaling both $\langle \mathcal{D}_s \rangle$ and σ by functions of k_0 results in complete overlapping of $\langle \mathcal{D}_s(\sigma) \rangle$ for different values of k_0 on intermediate to large scales but not on small scales. Numerical measurements of $\langle \mathcal{D}_s(\sigma) \rangle$ therefore indicate that k_0 sets the overall scale of the quantum geometry on sufficiently large scales but that k_0 does not set the overall scale of the quantum geometry on sufficiently small scales. While this conclusion is consistent with the findings of Ambjørn, Jurkiewicz, and Loll, confirmed just above, since $\langle N_2^{\text{SL}}(\tau) \rangle$ is a large-scale observable, this conclusion necessitates a refinement of these authors' conjecture. The breakdown of their conjecture is not unexpected: as evidenced by the dynamics of $\langle \mathcal{D}_s(\sigma) \rangle$, at least three scales—the rate of dynamical dimensional reduction, the scale associated with σ_{max} , and the rate of large-scale decay of $\langle \mathcal{D}_s(\sigma) \rangle$ —characterize the quantum geometry within phase C, of which only the last coincides with the overall scale of $\langle N_2^{\text{SL}}(\tau) \rangle$.

⁷I exclude the (presumably) unphysically small values of $\langle \mathcal{D}_s(\sigma) \rangle$ for very small values of σ ($\sigma < 15$ for $k_0 = 0.5$, $\sigma < 9$ for $k_0 = 1.0$, $\sigma < 7$ for $k_0 = 1.5$, $\sigma < 5$ for $k_0 = 2.0$, $\sigma < 5$ for $k_0 = 2.5$).

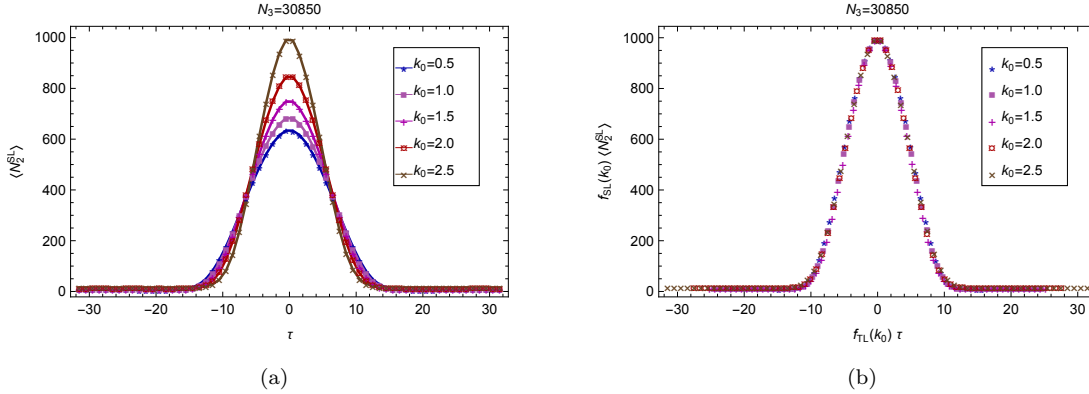


Figure 4.16: (a) The ensemble average number $\langle N_2^{\text{SL}} \rangle$ of spacelike 2-simplices as a function of the discrete time coordinate τ for five values of the bare coupling k_0 for $N_3 = 30850$ and $T = 64$. (b) The ensemble average number $f_{\text{SL}}(k_0) \langle N_2^{\text{SL}} \rangle$ of spacelike 2-simplices, scaled by the function $f_{\text{SL}}(k_0)$, as a function of the discrete time coordinate $f_{\text{TL}}(k_0) \tau$, scaled by the function $f_{\text{TL}}(k_0)$, for five values of the bare coupling k_0 for $N_3 = 30850$ and $T = 64$.

5 Conclusion

I have aimed to study comprehensively the phenomenology of the small-to-intermediate scale spectral dimension within phase C of the causal dynamical triangulations of 3-dimensional Einstein gravity. To this end I performed systematic numerical measurements of the ensemble average spectral dimension $\langle \mathcal{D}_s(\sigma) \rangle$ as a function of the diffusion time σ . I presented and analyzed these measurements in section 4, investigating the dependence of $\langle \mathcal{D}_s(\sigma) \rangle$ on the three parameters that enter into a measurement of $\langle \mathcal{D}_s(\sigma) \rangle$: the diffusion constant ρ , the number N_3 of 3-simplices, and the bare coupling k_0 . In subsection 4.1 I demonstrated that $\langle \mathcal{D}_s(\sigma) \rangle$ depends trivially on ρ : ρ simply rescales σ as equation (3.1), describing diffusion on a Riemannian manifold, implies. In subsection 4.2 I found that the maximal value $\langle \mathcal{D}_s \rangle_{\text{max}}$ of $\langle \mathcal{D}_s(\sigma) \rangle$ is finite in the infinite volume limit but that $\langle \mathcal{D}_s \rangle_{\text{max}}$ slightly overshoots the topological dimension of 3. In subsection 4.3 I found that the minimal value $\langle \mathcal{D}_s \rangle_{\text{min}}$ of $\langle \mathcal{D}_s(\sigma) \rangle$ —the value to which $\langle \mathcal{D}_s(\sigma) \rangle$ dynamically reduces—decreases with k_0 towards the AC phase transition. This last finding leads to the conclusion that k_0 alone does not set the scales of the quantum geometry on sufficiently small scales, counter to a conjecture of Ambjørn, Jurkiewicz, and Loll [11].

Taken together, the results of section 4 lead to several novel insights. The findings of subsections 4.2 and 4.3 point to the possibility of $\langle \mathcal{D}_s \rangle_{\text{max}}$ equaling 3 in the infinite volume limit. While $\langle \mathcal{D}_s \rangle_{\text{max}}$ clearly overshoots 3 in the infinite volume limit for $k_0 = 1.0$, $\langle \mathcal{D}_s \rangle_{\text{max}}$ decreases as k_0 approaches the AC phase transition for fixed N_3 . By adjusting k_0 to a value near k_0^c , I propose that $\langle \mathcal{D}_s \rangle_{\text{max}}$ would be precisely tuned to a value of 3 in the infinite volume limit. The quantum geometry of phase C would then exhibit exact (spectral) 3-dimensionality on the intermediate scale associated with σ_{max} . A finite-size scaling analysis of $\langle \mathcal{D}_s(\sigma) \rangle$ for $k_0 \lesssim k_0^c$ would readily test this proposal.

The findings of subsection 4.3 point to consistency with the spectral dimension within phase A. As Anderson *et al* first reported [15], $\langle \mathcal{D}_s(\sigma) \rangle$ within phase A is an approximately constant function of σ with a value of approximately $\frac{3}{2}$. Coumbe and Jurkiewicz subsequently measured $\langle \mathcal{D}_s(\sigma) \rangle$ within phase A of the causal dynamical triangulations of 4-dimensional Einstein gravity, finding that $\langle \mathcal{D}_s(\sigma) \rangle$ is an approximately constant function of σ with a value of approximately $\frac{4}{3}$ [26]. In fact, both of these measurements show $\langle \mathcal{D}_s(\sigma) \rangle$ decreasing very slowly with σ , presumably owing to the compact topology of each causal triangulation. I have measured $\langle \mathcal{D}_s(\sigma) \rangle$ for four values of k_0 within phase A (including the value of k_0 considered by Anderson *et al*). As these four measurements reveal very little variation of $\langle \mathcal{D}_s(\sigma) \rangle$ with k_0 , I plot in figure 5.1 just the case of $k_0 = 6.0$, which shows consistency with the measurement of [15]. Since Anderson *et al* and I measured $\langle \mathcal{D}_s(\sigma) \rangle$ for $k_0 = 6.0$ at $N_3 = 10240$, the value of approximately $\frac{3}{2}$ obtained might be depressed by finite-size effects in which case $\langle \mathcal{D}_s(\sigma) \rangle$ might approach a value of $\frac{4}{3}$ in the infinite volume limit.

Phase A is regarded as the analogue in causal dynamical triangulations of the branched polymeric phase of

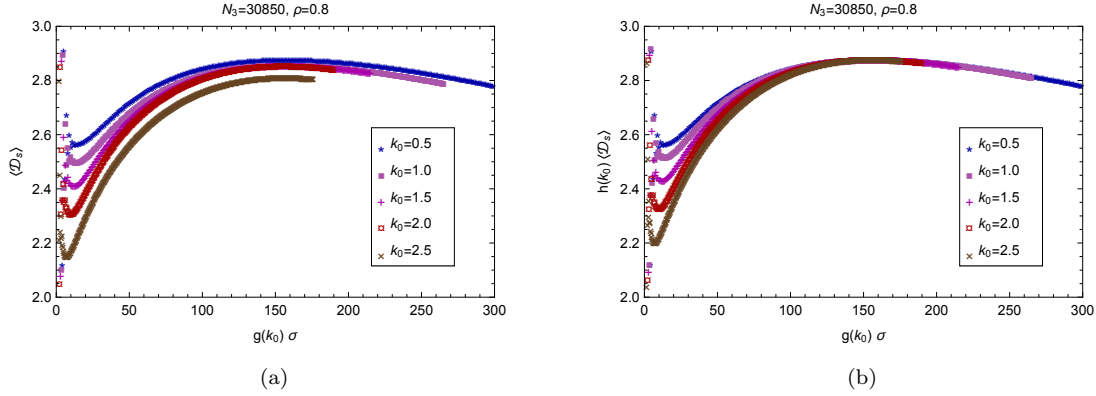


Figure 4.17: (a) The ensemble average spectral dimension $\langle \mathcal{D}_s \rangle$ as a function of the diffusion time $g(k_0)\sigma$, scaled by the function $g(k_0)$, for five values of the bare coupling k_0 for $N_3 = 30850$, $T = 64$, and $\rho = 0.8$. (b) The ensemble average spectral dimension $h(k_0)\langle \mathcal{D}_s \rangle$, scaled by the function $h(k_0)$, as a function of the diffusion time $g(k_0)\sigma$, scaled by the function $g(k_0)$, for five values of the bare coupling k_0 for $N_3 = 30850$, $T = 64$, and $\rho = 0.8$.

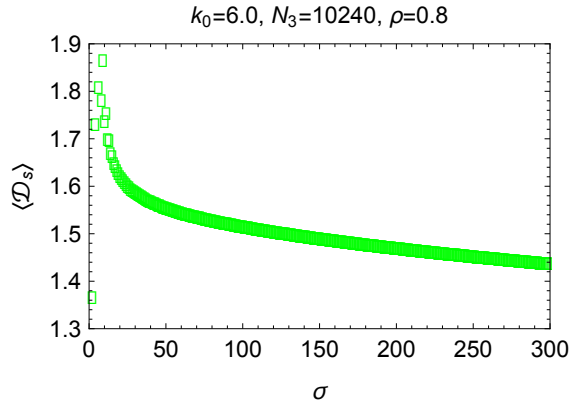


Figure 5.1: The ensemble average spectral dimension $\langle \mathcal{D}_s \rangle$ as a function of the diffusion time σ for $k_0 = 6.0$, $N_3 = 10240$, $T = 64$, and $\rho = 0.8$.

Euclidean dynamical triangulations [11, 13]. Branched polymers are self-similar or scale-invariant structures as evidenced, for instance, by the constancy of their spectral dimension with the diffusion time. Ordinary branched polymers have a spectral dimension of $\frac{4}{3}$ [27] while a novel class of branched polymers allows for a spectral dimension of $\frac{3}{2}$ [4, 5, 13]. The spectral dimension of phase A is therefore consistent with that of branched polymers.

I now attempt to reconcile the numerical measurements of $\langle \mathcal{D}_s(\sigma) \rangle$ within phase A with the findings of subsection 4.3. Extrapolating from figure 4.13, I hypothesize that $\langle \mathcal{D}_s \rangle_{\max}$ continues to decrease with k_0 towards a value of approximately $\frac{3}{2}$ at the AC phase transition. Extrapolating from figure 4.14, I hypothesize that σ_{\max} diverges as k_0 approaches k_0^c . Extrapolating from figure 4.15, I hypothesize that $\langle \mathcal{D}_s \rangle_{\min}$ continues to decrease with k_0 towards a value of approximately $\frac{3}{2}$ at the AC phase transition. Equivalently, I propose that $\langle \mathcal{D}_s(\sigma) \rangle$ changes continuously from its characteristic behavior in phase C, depicted in figures 4.1, 4.2, 4.6, 4.11, and 4.12, to its characteristic behavior in phase A, depicted in figure 5.1, as k_0 approaches k_0^c .

This hypothesized consistency of $\langle \mathcal{D}_s(\sigma) \rangle$ across the AC phase transition suggests a physical explanation for the dynamical reduction of $\langle \mathcal{D}_s(\sigma) \rangle$ observed within phase C: on sufficiently small scales the quantum geometry of phase C is branched polymeric. In particular, the decrease in $\langle \mathcal{D}_s \rangle_{\min}$ with k_0 would halt at a value of approximately $\frac{3}{2}$, fixed by the branched polymeric nature of the quantum geometry on sufficiently small scales. This explanation's viability clearly rests on the findings of future investigations, for instance,

of the type performed in [13]. This explanation itself suggests that ensembles of causal triangulations closer to the AC phase transition probe smaller physical scales for fixed N_3 . An analysis of the type performed in [24] might test this suggestion.

This physical explanation of dynamical dimensional reduction also harmonizes with the aim of causal dynamical triangulations. As I briefly discussed at the end of section 2, one hopes to remove the regularization by causal triangulations by taking a continuum limit at a nontrivial ultraviolet fixed point. The theory corresponding to a fixed point is scale-invariant, and, as I noted just above, branched polymers are scale-invariant structures. Branched polymeric quantum geometry on sufficiently small scales could thus signal the existence of the desired fixed point.

To determine whether a continuum limit exists, one typically performs a renormalization group analysis. Specifically, one looks for renormalization group trajectories connected to a candidate fixed point location along which the lattice spacing approaches zero (in physical units) as the trajectories approach this location. If such trajectories exist, then one can take a continuum limit by tuning the bare couplings to the fixed point. Such an analysis assumes that one knows how to delineate renormalization group flows. In most contexts—specifically, those in which there is a fixed spacetime—this assumption is completely justified: there exist well-established techniques for delineating renormalization group flows, for instance, coarse-graining transformations or flow equations. In the context of nonperturbative quantum theories of gravity—in which case there is no fixed spacetime—delineating renormalization group trajectories is considerably more difficult [19]. How does one delineate a renormalization group trajectory in the latter context? As Ambjørn *et al* and Cooperman clearly explain [6, 21], one must return to the defining characteristic of a renormalization group trajectory: the physics described by the succession of effective theories along a renormalization group trajectory remains fixed, merely being probed over different intervals of scales. Accordingly, one delineates a renormalization group trajectory by following fixed values of sufficiently many physical observables through the space of effective theories as the interval of scales being probed changes systematically. Of course, coarse-graining transformations and flow equations employ this definition, but their presentations and implementations do not always make this methodology apparent. How does one change the interval of scales being probed in the latter context? At least within causal dynamical triangulations, as Ambjørn *et al* [6] and Cooperman also clearly explain [6, 21], one directly simulates ensembles of causal triangulations intrinsically characterized by different intervals of scales.

Ambjørn *et al* and Cooperman both proposed renormalization group schemes for causal dynamical triangulations on this basis; however, their schemes were too deficient in physical observables to allow for unambiguous delineation of renormalization group trajectories [6, 21]. To overcome this deficiency, Ambjørn *et al* invoked an additional assumption, a constant lattice spacing [6], whereas Cooperman proposed employing an additional physical observable, the spectral dimension [21]. The value of the spectral dimension at a fixed physical scale—as opposed to its value at a fixed diffusion time—is a physical observable. One could therefore use the spectral dimension in delineating renormalization group trajectories provided that one could also determine the physical scale at which the spectral dimension takes a specified value. Making this determination proves rather nontrivial, but I am currently pursuing this goal [23]. Since one simulates different ensembles of causal triangulations to change the interval of scales being probed, using the spectral dimension to delineate renormalization group trajectories translates into determining the circumstances under which measurements of $\langle \mathcal{D}_s(\sigma) \rangle$ on different ensembles probe the same spectral dimension. Understanding the dependence of $\langle \mathcal{D}_s(\sigma) \rangle$ on the number of D -simplices and the bare couplings is crucial to making this determination.

Acknowledgements

I thank Christian Anderson, Jonah Miller, and especially Rajesh Kommu for allowing me to employ parts of their codes. I am indebted to Jonah Miller for providing computing facilities on which to run some of my codes. I also thank Jan Ambjørn, Steve Carlip, Daniel Coumbe, Hal Haggard, Joe Henson, and Renate Loll for useful discussions. I acknowledge the hospitality of the Physics Program of Bard College where I completed much of this research.

A Estimates and errors

I estimate the ensemble average spectral dimension $\langle \mathcal{D}_{\mathfrak{s}}(\sigma) \rangle$ and the error $\epsilon[\langle \mathcal{D}_{\mathfrak{s}}(\sigma) \rangle]$ in $\langle \mathcal{D}_{\mathfrak{s}}(\sigma) \rangle$ as follows [20]. Since the number N_3 of 3-simplices is on the order of 10^5 or 10^6 for the causal triangulations \mathcal{T}_c that I have simulated, I cannot feasibly compute the return probability $\mathcal{P}_{\mathcal{T}_c}(\sigma)$ by summing the heat kernel elements $\mathcal{K}_{\mathcal{T}_c}(\mathfrak{s}, \mathfrak{s}, \sigma)$ over every 3-simplex \mathfrak{s} in \mathcal{T}_c . I instead estimate $\mathcal{P}_{\mathcal{T}_c}(\sigma)$ by sampling a subset of M randomly selected 3-simplices \mathfrak{s}_m :

$$\mathcal{P}_{\mathcal{T}_c}^{(M)}(\sigma) = \frac{1}{M} \sum_{\mathfrak{s}_m \in \mathcal{T}_c} \mathcal{K}_{\mathcal{T}_c}(\mathfrak{s}_m, \mathfrak{s}_m, \sigma). \quad (\text{A.1})$$

I then estimate the spectral dimension $\mathcal{D}_{\mathfrak{s}}^{(\mathcal{T}_c)}(\sigma)$ as follows:

$$\mathcal{D}_{\mathfrak{s}}^{(\mathcal{T}_c, M)}(\sigma) = -\frac{\sigma}{\mathcal{P}_{\mathcal{T}_c}^{(M)}(\sigma)} \left[\mathcal{P}_{\mathcal{T}_c}^{(M)}(\sigma + 1) - \mathcal{P}_{\mathcal{T}_c}^{(M)}(\sigma - 1) \right]. \quad (\text{A.2})$$

By sampling a subset of M 3-simplices, I induce an error $\epsilon[\mathcal{D}_{\mathfrak{s}}^{(\mathcal{T}_c, M)}(\sigma)]$ in $\mathcal{D}_{\mathfrak{s}}^{(\mathcal{T}_c, M)}(\sigma)$. I estimate $\epsilon[\mathcal{D}_{\mathfrak{s}}^{(\mathcal{T}_c, M)}(\sigma)]$ as follows. I compute the M jackknife estimates of $\mathcal{P}_{\mathcal{T}_c}^{(M)}(\sigma)$,

$$\mathcal{P}_{\mathcal{T}_c}^{(M_l)}(\sigma) = \frac{1}{M-1} \sum_{\substack{\mathfrak{s}_m \in \mathcal{T}_c \\ m \neq l}} \mathcal{K}(\mathfrak{s}_m, \mathfrak{s}_m, \sigma), \quad (\text{A.3})$$

and the M corresponding jackknife estimates of $\mathcal{D}_{\mathfrak{s}}^{(\mathcal{T}_c, M)}(\sigma)$,

$$\mathcal{D}_{\mathfrak{s}}^{(\mathcal{T}_c, M_l)}(\sigma) = -\frac{\sigma}{\mathcal{P}_{\mathcal{T}_c}^{(M_l)}(\sigma)} \left[\mathcal{P}_{\mathcal{T}_c}^{(M_l)}(\sigma + 1) - \mathcal{P}_{\mathcal{T}_c}^{(M_l)}(\sigma - 1) \right], \quad (\text{A.4})$$

both for $l \in \{1, \dots, M\}$. I take $\epsilon[\mathcal{D}_{\mathfrak{s}}^{(\mathcal{T}_c, M)}(\sigma)]$ as the jackknife error in $\mathcal{D}_{\mathfrak{s}}^{(\mathcal{T}_c, M)}(\sigma)$:

$$\epsilon[\mathcal{D}_{\mathfrak{s}}^{(\mathcal{T}_c, M)}(\sigma)] = \sqrt{\frac{M-1}{M} \sum_{l=1}^M \left[\mathcal{D}_{\mathfrak{s}}^{(\mathcal{T}_c, M_l)}(\sigma) - \mathcal{D}_{\mathfrak{s}}^{(\mathcal{T}_c, M)}(\sigma) \right]^2}. \quad (\text{A.5})$$

Since the number of causal triangulations at fixed N_3 grows tremendously with N_3 , I can only feasibly simulate a finite number $N(\mathcal{T}_c)$ of causal triangulations. I instead estimate the ensemble average spectral dimension $\langle \mathcal{D}_{\mathfrak{s}}(\sigma) \rangle$ as follows:

$$\langle \mathcal{D}_{\mathfrak{s}}^{(M)}(\sigma) \rangle = \frac{1}{N(\mathcal{T}_c)} \sum_{j=1}^{N(\mathcal{T}_c)} \mathcal{D}_{\mathfrak{s}}^{(\mathcal{T}_c^{(j)}, M)}(\sigma). \quad (\text{A.6})$$

By sampling a subset of $N(\mathcal{T}_c)$ causal triangulations, I induce an error $\epsilon[\langle \mathcal{D}_{\mathfrak{s}}(\sigma) \rangle]$ in $\langle \mathcal{D}_{\mathfrak{s}}(\sigma) \rangle$. I take $\epsilon[\langle \mathcal{D}_{\mathfrak{s}}(\sigma) \rangle]$ as the standard error in $\langle \mathcal{D}_{\mathfrak{s}}(\sigma) \rangle$:

$$\epsilon[\langle \mathcal{D}_{\mathfrak{s}}(\sigma) \rangle] = \sqrt{\frac{1}{N(\mathcal{T}_c)[N(\mathcal{T}_c) - 1]} \sum_{j=1}^{N(\mathcal{T}_c)} \left[\mathcal{D}_{\mathfrak{s}}^{(\mathcal{T}_c^{(j)}, M)}(\sigma) - \langle \mathcal{D}_{\mathfrak{s}}^{(M)}(\sigma) \rangle \right]^2} \quad (\text{A.7})$$

I take the total error as

$$\langle \epsilon[\mathcal{D}_{\mathfrak{s}}^{(M)}(\sigma)] \rangle + \epsilon[\langle \mathcal{D}_{\mathfrak{s}}(\sigma) \rangle] \quad (\text{A.8})$$

in which

$$\langle \epsilon[\mathcal{D}_{\mathfrak{s}}^{(M)}(\sigma)] \rangle = \frac{1}{N(\mathcal{T}_c)} \sqrt{\sum_{j=1}^{N(\mathcal{T}_c)} \epsilon^2[\mathcal{D}_{\mathfrak{s}}^{(\mathcal{T}_c^{(j)}, M)}(\sigma)]}, \quad (\text{A.9})$$

the error propagated to $\langle \mathcal{D}_{\mathfrak{s}}(\sigma) \rangle$ from $\mathcal{D}_{\mathfrak{s}}^{(\mathcal{T}_c, M)}(\sigma)$ in computing the ensemble average.

References

- [1] J. Ambjørn, D. N. Coumbe, J. Gizbert-Studnicki, A. Görlich, and J. Jurkiewicz. “New higher-order transition in causal dynamical triangulations.” *Physical Review D* 95 (2017) 124029.
- [2] J. Ambjørn, D. N. Coumbe, J. Gizbert-Studnicki, A. Görlich, J. Jurkiewicz, N. Klitgaard, and R. Loll. “Characteristics of the new phase in CDT.” *European Physical Journal C* 77 (2017) 152.
- [3] J. Ambjørn, D. N. Coumbe, J. Gizbert-Studnicki, and J. Jurkiewicz. “Searching for a continuum limit of causal dynamical triangulation quantum gravity.” *Physical Review D* 93 (2016) 104032.
- [4] J. Ambjørn, B. Durhuus, B. Durhuus, and T. Jonsson. “A solvable 2D quantum gravity model with $\gamma > 0$.” *Modern Physics Letters A* 9 (1994) 1221.
- [5] J. Ambjørn, B. Durhuus, T. Jonsson, and G. Thorleifsson. “Matter fields with $c > 1$ coupled to 2d gravity.” *Nuclear Physics B* 398 (1993) 568.
- [6] J. Ambjørn, A. Görlich, J. Jurkiewicz, A. Kreienbuehl, and R. Loll. “Renormalization group flow in CDT.” *Classical and Quantum Gravity* 31 (2014) 165003.
- [7] J. Ambjørn, S. Jordan, J. Jurkiewicz, and R. Loll. “Second-Order Phase Transition in Causal Dynamical Triangulations.” *Physical Review Letters* 107 (2011) 211303.
- [8] J. Ambjørn, S. Jordan, J. Jurkiewicz, and R. Loll. “Second- and first-order phase transitions in causal dynamical triangulations.” *Physical Review D* 85 (2012) 124044.
- [9] J. Ambjørn, J. Jurkiewicz, and R. Loll. “Non-perturbative Lorentzian Path Integral for Gravity.” *Physical Review Letters* 85 (2000) 347.
- [10] J. Ambjørn, J. Jurkiewicz, and R. Loll. “Dynamically triangulating Lorentzian quantum gravity.” *Nuclear Physics B* 610 (2001) 347.
- [11] J. Ambjørn, J. Jurkiewicz, and R. Loll. “Nonperturbative 3d Lorentzian Quantum Gravity.” *Physical Review D* 64 (2001) 044011.
- [12] J. Ambjørn, J. Jurkiewicz, and R. Loll. “The Spectral Dimension of the Universe is Scale Dependent.” *Physical Review Letters* 95 (2005) 171301.
- [13] J. Ambjørn, J. Jurkiewicz, and R. Loll. “Reconstructing the universe.” *Physical Review D* 72 (2005) 064014.
- [14] J. Ambjørn and R. Loll. “Non-perturbative Lorentzian quantum gravity, causality, and topology change.” *Nuclear Physics B* 536 (1998) 407.
- [15] C. Anderson, S. Carlip, J. H. Cooperman, P. Hořava, R. K. Kommu, and P. Zulkowski. “Quantizing Hořava-Lifshitz gravity via causal dynamical triangulations.” *Physical Review D* 85 (2012) 049904.
- [16] D. Benedetti and J. Henson. “Spectral geometry as a probe of quantum spacetime.” *Physical Review D* 80 (2009) 124036.
- [17] D. Benedetti and J. Henson. “Spacetime condensation in (2+1)-dimensional CDT from a Hořava-Lifshitz minisuperspace model.” *Classical and Quantum Gravity* 32 (2015) 215007.
- [18] S. Carlip. “Dimension and dimensional reduction in quantum gravity.” *Classical and Quantum Gravity* 34 (2017) 193001.
- [19] J. H. Cooperman. “Renormalization of lattice-regularized quantum gravity models I. General considerations.” arXiv: 1410.0026.
- [20] J. H. Cooperman. “Scale-dependent homogeneity measures for causal dynamical triangulations.” *Physical Review D* 90 (2014) 124053.

- [21] J. H. Cooperman. “On a renormalization group scheme for causal dynamical triangulations.” *General Relativity and Gravitation* 48 (2016) 1.
- [22] J. H. Cooperman. “Comments on ‘Searching for a continuum limit in CDT quantum gravity’.” arXiv: 1604.01798
- [23] J. H. Cooperman and M. Dorghabekov. “Setting the scale of dynamical dimensional reduction in causal dynamical triangulations.” In preparation.
- [24] J. H. Cooperman, K. Lee, and J. M. Miller. “A second look at transition amplitudes in (2+1)-dimensional causal dynamical triangulations.” *Classical and Quantum Gravity* 34 (2017) 115008.
- [25] J. H. Cooperman and J. M. Miller. “A first look at transition amplitudes in (2 + 1)-dimensional causal dynamical triangulations.” *Classical and Quantum Gravity* 31 (2014) 035012.
- [26] D. N. Coumbe and J. Jurkiewicz. “Evidence for asymptotic safety from dimensional reduction in causal dynamical triangulations.” *Journal of High Energy Physics* 03 (2015) 151.
- [27] T. Jonsson and J. F. Wheeler. “The spectral dimension of the branched polymers phase of two-dimensional quantum gravity.” *Nuclear Physics B* 515 (1998) 549.
- [28] R. K. Kommu. “A validation of causal dynamical triangulations.” *Classical and Quantum Gravity* 29 (2012) 105003.